Published in final edited form as:
Med Sci Monit. 2008 July ; 14(7): CR345–CR352.

Temporal clustering analysis: What does it tell us about the resting state of the brain?

Victoria L. Morgan[1,A,B,C,D,E,F,G], **John C. Gore**[1,A,B,D,E,F,G], and **Jerzy P. Szaflarski**[2,A,B,D,E,F,G]

1*Vanderbilt University Institute of Imaging Science and the Department of Radiology and Radiological Sciences, Vanderbilt University, Nashville, TN, U.S.A.*

2*University of Cincinnati Academic Health Center, Departments of Neurology and Neuroscience, Center for Imaging Research and The Neuroscience Institute, Cincinnati, OH, U.S.A.*

Abstract

Background—Several networks of synchronous blood oxygen level dependent (BOLD) oscillations have been identified in the brain during the resting state. The aim of this study was to further characterize the dynamic nature of the brain at rest by investigating the presence and distribution of coherent, transient BOLD activity in resting fMRI data using a novel method of fMRI data analysis - 2dTCA.

Material/Methods—High-field fMRI data were acquired in 27 subjects. The temporal clustering analysis, 2dTCA, was implemented to determine the timing of significant, spatially coherent, transient BOLD signal changes. Group maps of positive and negative coherent BOLD changes from each timing profile were created.

Results—Spontaneous increases in BOLD activity at both 3T and 4T and decreases at 4T were found in regions of the alpha rhythm circuit including the thalamus, precuneus and the occipital cortex. Additional positive and negative oscillations at 4T and a small region of positive activity at 3T were identified in the area of the brain stem reticular formation, the control center for maintaining arousal and motivation.

Conclusions—These results provide additional evidence for the presence of dynamic functional networks in the resting brain that are active while the subjects appear to be at rest and that are spatially distributed in areas responsible for maintaining consciousness and vigilance including brain stem. These findings should be considered in interpreting fMRI results which use resting baseline for comparisons.

Keywords

functional MRI; consciousness; vigilance; thalamus; neuroimaging; biological rhythms and sleep; brain stem

Correspondence to: Jerzy P. Szaflarski.

Author's address: Jerzy P. Szaflarski, MD, PhD, University of Cincinnati Academic Health Center, Department of Neurology, 260 Stetson Street Rm. 2350, Cincinnati, OH 45267-0525, U.S.A., e-mail: Jerzy.Szaflarski@uc.edu.

[A]Authors' Contributions:
Study Design
[B]Data Collection
[C]Statistical Analysis
[D]Data Interpretation
[E]Manuscript Preparation
[F]Literature Search
[G]Funds Collection

Background

Neuroimaging investigations of brain function frequently incorporate comparisons between baseline or control and active conditions. Although frequently called a “resting” condition, the state of the brain during such periods is far from quiescent. In fact, it is known that the resting state of the brain, usually defined as wakefulness with either eyes closed or with visual fixation, consumes relatively large amounts of energy, much of which is associated with neural activity. At rest, the brain accounts for approximately 20% of the total body oxygen consumption utilized primarily to maintain glutamatergic and GABA-related neurotransmission [1,2]. There is evidence that this baseline neural activity and its effect on the results of neuroimaging studies incorporating rest as a control condition may be significant and related to working memory, executive functions, episodic memory, and semantic processing [3-7].

Resting state functional connectivity measurements identify regions of the brain that are functionally coupled (i.e., networked). It is hypothesized that components of such a network will have synchronous low frequency fluctuations of baseline neural activity visualized in neuroimaging studies as changes in the proportions of oxy- and deoxyhemoglobin producing oscillations of the blood oxygen level dependent (BOLD) fMRI signal [8,9]. These resting state correlations have been found across various systems including the motor cortex [10], the visual cortex [11] and the language pathways [12]. Other work has described not only positively correlated networks, but complementary activations and deactivations within the networks with corresponding increases in BOLD signal in one part and decreases in another part of the network [13,14]. Also, this connectivity has been found to be modulated by task load [11,15] and disease [16,17]. Although these studies have provided us with detailed information regarding the state of certain regions of the brain in the resting period, generalization of the results has been difficult because many of these studies use pre-defined seed regions requiring *a priori* hypotheses regarding these regions.

In contrast to the other methods requiring *a priori* hypothesis regarding the specific brain regions involved in an examined process, independent component analysis (ICA) is a data driven analysis method that does not involve the use of pre-defined regions of interest. ICA is used to separate the fMRI data into independent components based on the assumption that these individual contributions (including physiological signals, noise and artifacts) are statistically independent and combine linearly to create the observed signal [18]. Prior application of ICA to the analysis of the resting fMRI data has revealed multiple networks that appear to be active during the so-called resting state [19-21]. Like the ones studied with functional connectivity, these networks include regions involved in primary motor and sensory processing, executive functioning, memory and vigilance. These studies have also been used to identify the so-called default-mode network. This network includes the posterior cingu-late, the ventral anterior cingulate, and the bilateral inferior parietal cortices [22]. It is postulated that this network supports the baseline attention state of the brain at rest. In healthy subjects, these regions are deactivated (negative BOLD signal changes) using a task-rest paradigm and exhibit an increase in oxygen extraction fraction at rest [22]; these regions are functionally connected at rest and during some passive sensory processing [22,23].

In view of the results of the previous studies, we hypothesize that, in comparison to the known resting networks described above, novel regions of coherent resting state BOLD activity may be detected using a signal processing method called temporal clustering analysis (TCA) [24-27]. This algorithm is a data-driven method that does not require *a priori* hypotheses and, therefore, it can be used to determine the temporal profile of voxels experiencing significant and simultaneous transient, positive or negative BOLD signal changes. Recently, we have adapted the original TCA method to the detection of the transient BOLD signal changes

resulting from interictal epileptiform activity in patients with temporal lobe epilepsy [28] and developed a two-dimensional variation of the original TCA method called 2dTCA in an to attempt to separate signals from different sources [29,30]. Therefore, the aim of this study was to investigate the presence of coherent transient BOLD signal changes in the brain's resting state by applying 2dTCA to high field resting fMRI data.

Material and Methods

Subjects

Data were acquired in two separate studies at two institutions. In one study, 12 healthy control subjects (6M, 6F, mean age ±stdev: 27.8±5 years) were recruited and imaged at Vanderbilt University (*3T dataset*). In a second study, 15 healthy controls (10M, 5 F, mean age ±stdev: 32.8±9 years) were recruited and imaged at the Center for Imaging Research, University of Cincinnati Academic Health Center (*4T dataset*). All subjects were free of any neurological, psychiatric or medical conditions as determined by interview. Informed consent was obtained prior to scanning in accordance with Institutional Review Board guidelines of each institution.

MRI scanning

3T dataset—MRI imaging was performed using a Philips Achieva 3T MRI scanner (Philips Medical Systems, Inc, Best, Netherlands) with an 8-channel SENSE coil. Scanning included a two-dimensional, Tl-weighted high-resolution image set covering the whole brain (256×256, FOV = 240 mm, 4.5 mm thick/0.5 mm gap, 30 axial slices); a three-dimensional, T1-weighted high-resolution whole brain image set (256×256×170, FOV = 256 mm, 1×1×1 mm, axial) for spatial normalization; and one T2*-weighted gradient-echo, echo planar BOLD fMRI scan with subject instructed to hold still with eyes closed. Imaging parameters are in Table 1.

4T dataset—Images were acquired using a Varian Unity INOVA 4T MRI scanner (Varian, Inc, Palo Alto, CA) while simultaneously acquiring EEG information with a 64 channel MRI-compatible EEG system (Compumedics Neuroscan, Inc, El Paso, TX). A three-dimensional, Tl-weighted high resolution image set (192×256×192, FOV = 256, 1×1×1 mm, axial) and one or two T2*-weighted echo planar BOLD fMRI series at rest with eyes closed were acquired from each subject. Music of personal choice was played through headphones throughout the scanning. Only the first fMRI scan acquired from each subject was analyzed for this study. See Table 1 for imaging parameters. EEG analyses are not included here.

Image analysis

The 3T and 4T datasets were analyzed separately in the same manner except where noted. The data were preprocessed using SPM5 [http://www.fil.ion.ucl.ac.uk/spm/spm5.html] image processing software including correction for slice timing effects due to the interleaved image acquisition, and realignment to the first volume in each series to correct for head motions. Then, each subject's fMRI images were spatially normalized to the MNI template [31] using SPM5. All fMRI datasets were then interpolated to 4×4×4 mm (47×56×46 voxels) and temporally smoothed using a three-point average. Intensity values were normalized to the first five time points of the voxel to determine percent signal change at each time point.

The next step of data analysis was to apply 2dTCA to the resting fMRI data in order to search for significant coherent, transient BOLD signal changes. First, we determined the global time course for all voxels based on the average time course from voxels that were not expected to contain a significant transient BOLD signal change (i.e., voxels in brain areas that are not thought to be part of the investigated networks and that are expected not to show any substantial BOLD signal oscillations related to changes in vigilance). These “quiescent” voxels were defined as those whose (1) maximum percent signal change was not within pre-determined

signal change limits expected by the BOLD response, and (2) maximum was less than two standard deviations above the mean of that voxel's signal through time (did not experience a significant signal increase). This global time course was subtracted from all voxel time courses to decrease global signal changes such as baseline drift and motion. Each voxels' time course was further corrected for low frequency noise using detrending. All datasets were then concatenated to perform the next step, a group clustering analysis.

Under the assumption that the above preprocessed data should contain temporal noise that is now generally randomly distributed, significant signal changes through time can be denned as times where the signal is two standard deviations from the mean. To perform the 2dTCA clustering analysis, time points of simultaneous, transient BOLD signal changes were identified for each individual voxel that had at least one time point whose maximum intensity was at least two standard deviations above the mean through time. This was done by creating a two-dimensional mapping of each voxel time course, *Z(1: N)* (where N = number of time points in one BOLD series * number of subjects in group), into an *N* by *N* matrix, *hist2d*, by incrementing the values in the following manner for all voxels:

$$For\ Z(y)_{y=1\,to\,N},\ \mathrm{hist2}d\,(x,y) = \begin{cases} \mathrm{hist2}d\,(x,y)+1,\ if\ Z\,(y) \geq \mathrm{threshold} \\ \mathrm{hist2}d\,(x,y)+0,\ if\ Z\,(y) < \mathrm{threshold} \end{cases}$$

where threshold = mean(Z) + 1.5*standard deviation(Z) and $x = \min(y)$ at which $Z\,(y) \geq$ threshold. Therefore, the x-axis of *hist2d* is the time of first significant signal increase and the y-axis is the time at each significant signal increase of the time course. In this way, each column of the matrix consists of the histogram of significant signal increases for those voxels whose first time point exceeding the threshold occurred at time point *x* (Figure 1) [29,30]. This is in contrast to the one-dimensional histogram mapping (*hist1d*(1: *N*)) of the original TCA method [25,28]:

$$For\ Z(y)_{y=1\,to\,N},\ \mathrm{hist1}d\,(y) = \begin{cases} \mathrm{hist1}d\,(y)+1,\ if\ Z\,(y) = \max\,(Z) \\ \mathrm{hist1}d\,(y)+0,\ if\ Z\,(y) < \max\,(Z) \end{cases}$$

We chose 1.5 standard deviations over the mean through time as the threshold for a signal increase in an attempt to identify multiple signal change events (in addition to the maximum). However, only voxels whose maximum was at least two standard deviations above the mean were included in the mapping. These thresholds have been chosen specifically for this application but may be modified for other analyses.

This clustering resulted in *hist2d*(1: *N*,1: *N*) which can be considered *N* histograms (one from each column representing each different timing profile) of length *N* points each. Next, the specific columns of *hst2d* which indicate transient BOLD signals of interest were selected. To determine the most significant histograms, the diagonal of *hst2d*(1: *N*,1: *N*) was considered. Any points on the diagonal that exceed a given threshold were selected as indicators of times at which many voxels first experienced a significant signal increase. The corresponding columns of *hist2d* were then determined to be relevant histograms representing the timing profiles of interest. Further, any histograms that share at least 50% of their times of signal increases were added together to reduce the number of significant timing profiles.

Each resulting histogram (column) was considered a reference time course (RTC) indicating times of simultaneous, significant BOLD signal increase for some cluster of voxels across all subjects in the group. Each RTC was normalized by subtracting the mean and dividing by the standard deviation to indicate magnitude of signal change independent of the number of voxels that were used to find the cluster. The normalized RTCs and the global time course (calculated above) were used for each subject as regressors in the general linear model in a first-level, fixed-effects analysis. The result of this analysis was a contrast image for each subject for each

RTC. Each voxel value in the contrast image reflects the linear relationship between the RTC and the voxel time course of that subject.

In the final step, we performed a second-level analysis (one-sample t-test) using the contrast image corresponding to the same RTC across all subjects. This was repeated for each reference time course. Therefore, the final results were a group *t*-map for each RTC determined by the 2dTCA algorithm. The *t*maps were thresholded at $p<0.001$ with a cluster size of 5 (approximately $p<0.05$ corrected for multiple comparisons based on AlphaSim software [32]).

To identify regions of activation, the MNI coordinates of activated clusters were converted to Talairach coordinate estimates using a SPM5 supplied function (mni2tal.m, http://imaging.mrc-cbu.cam.ac.uk/imaging/MNITalairach). These Talairach coordinate estimates were then identified in the brain using a standard Talairach atlas [31].

The 2dTCA analysis was performed across subjects for each of the 3T and 4T datasets. Similarly, the timing of negative transient BOLD changes (deactivations) were also determined by multiplying the time course of each voxel by (−1) before implementing the 2dTCA clustering algorithm. First-level maps were then created using a negative contrast definition. Second-level t-tests were performed in the same way as the positive analyses.

Frequency analysis

For each RTC determined by the 2dTCA algorithm that produced an activation map at the $p<0.05$ (corrected for multiple comparisons) level, the power spectral density (PSD) was calculated using the fast Fourier transform. The PSD of each RTC was averaged across subjects to yield an average PSD for each reference time course.

Results

BOLD signal increases (activations)

The 2dTCA algorithm applied to the 3T dataset yielded one RTC (one activation map). This is shown in Figure 2A (white). Four RTCs were determined when the 2dTCA algorithm was applied to the 4T dataset which gave four activation maps. These are shown in Figure 2A (red, blue and green) and Figure 2B (red). The similarities between the regions of positive BOLD signal changes determined in the 3T and 4T datasets are illustrated in Figure 2A and are described in Table 2.

BOLD signal decreases (deactivations)

The 2dTCA algorithm detected one significant ($p<0.05$) RTC of coherent negative BOLD signal changes in the 3T dataset (Figure 3A; white). Six significant negative RTCs were detected from the 4T dataset. These are shown in Figure 3A (red, blue and green) and Figure 3B (red, blue and green). The similarities between these 3T and 4T negative activation maps and the positive activation maps are indicated in Figure 3A and in Table 2.

The average power spectral density plots across subjects are given in Figure 4. These data are organized in the same manner as Figures 2 and 3 with Figures 2AB,3A, and 3B map colors corresponding to line colors on Figure 4A,B,C,D, respectively. The maximum power in the positive 3T results was 0.0059 Hz, while all other PSDs in 3T and 4T datasets had peak power at approximately 0.002 Hz. However, other peaks were present across the lower frequencies (<0.10 Hz).

Discussion

Using the 2dTCA algorithm, several similar regions of resting coherent positive and negative BOLD signal changes were detected and localized in both 3T and 4T datasets. As indicated in Table 2 and in Figure 2A, the single map of 3T positive signal changes shared most regions of activation with the four 4T maps including the inferior parietal lobes, precuneus, thalamus, brainstem, occipital lobe, cerebellum and posterior cingulate. Many of these same regions showed coherent negative BOLD changes in the single 3T map and several 4T maps (Figure 3A), as well. In both the positive and negative cases, however, the 4T maps included more extensive activation than the 3T which is not surprising and quite expected as additional gains in BOLD signal strength are expected with increases in the strength of the magnet [33,34].

Interestingly, the regions of similarity between the 3T and 4T maps do not closely agree with those maps determined using another data-driven method, ICA [19-21], although are similar to those regions detected by others [4] when comparing rest and simple baseline tasks. However, one can interpret these findings by considering literature on modulation of EEG alpha rhythm in the brain. Alpha waves, in the frequency range of 8-13 Hz, occur during periods of resting wakefulness with eyes closed and are believed to be the result of internally driven cognitive stimuli to maintain awareness such as short term memory [35,36]. This rhythm could be the primary component of neural activity in our study.

Some simultaneous EEG and PET studies of the dominant alpha rhythm fluctuations showed negative correlations within the thalamus [37-39] while others found these correlations to be positive [40]. Positive correlations were also noted in the occipital cortex and the precuneus [41]. Combined EEG and fMRI studies yielded conflicting results. Some studies, in response to dominant alpha rhythm modulation, documented positive BOLD signal changes in thalamus and negative changes in the occipital and parietal regions [42,43]. Others found no correlation between the dominant alpha rhythm and thalamic activity, but negative BOLD signal changes in the parietal and frontal brain regions [44]. Two recent studies have attempted to explain these discrepancies by finding multiple maps of alpha involving these regions based on brain state and alpha frequency [45,46]. Finally, a most recent study focusing on this issue found that the thalamic response differs from the cortical response in amplitude and timing - a potential explanation for the differences found in these studies [47]. While mixed, these studies support the theory, first determined by electrophysiological studies, that the generation of alpha waves involves thalamocortical networks [35,36,40]. Specifically, our positive activation in the thalamus, occipital lobe and parietal regions may reflect transient BOLD activity in the network that controls alpha rhythm modulation.

In addition, there is evidence of concurrent modulation of the alpha rhythm by the cortico-subcortical networks. The pontine activation (Figure 2A) is consistent with the blink-alpha circuit which is believed to control both cycblink rate and alpha rhythm [48]. This circuit begins in the rostral pons and continues to subcortical midbrain structures and the occipital cortex. The brainstem structures in 4T map #4, 4Tmap#2 and a small part of 3T map#1 of positive changes (Figure 2A) and 4T map#3 of negative changes (Figure 3A) may also be considered regions of the brain stem reticular formation. This set of neurons modulates wakefulness, sleep and consciousness by controlling the flow of sensory information to many structures including the thalamus, hippocampus, hypothalamus and cerebellum. In animal studies, these brain stem areas have been shown to generate enhanced alpha frequency signals [36,49] and so they may be considered a part of the alpha circuit expressing its modulatory effect on thalamus and, therefore, resting state of the brain. The fact that the maps including these brainstem regions also include other regions believed to be a part of the alpha circuit supports this notion.

Recently, Feige et al. found activation in the anterior mid-brain near the substantia nigra in response to alpha modulation after reducing the BOLD hemodynamic delay from the standard 6 seconds to about 2.5 seconds [50]. This suggests that the subcortical activation may actually precede the detected occipital scalp EEG in time, explaining why it was not detected using standard methods in the previous neuroimaging studies of alpha rhythm generators. However, the coherent BOLD signal changes in the reticular formation may also be a result of independent external stimuli such as the sound of the scanner and/or music, the physical feel of the scanner bed and head coil, or the change of wakefulness or attentiveness of the subject during scanning. Concurrent to the positive BOLD signal changes, we noted significant BOLD signal decreases in the alpha modulating regions and reticular formation with clear overlap between the 3T and 4T datasets in the posterior cingulate and precuneus, which are part of the brain's default-mode network [22,23].

The frequency analysis shows maximum power at very low frequencies (<0.10 Hz) like those signals expected to reflect spontaneous oscillations of oxyhemoglobin and deoxy-hemoglobin detected using near infrared spectroscopy (NIRS) at rest [8]. The 3T dataset, with its higher temporal resolution and shorter scan time, showed power spread across a slightly larger range of frequencies than the 4T dataset. All of the 4T maps showed very similar frequency distributions. These results imply that (1) the signals detected with 2dTCA at rest arise from similar mechanisms as those used in the measurement of functional connectivity, and (2) that higher temporal resolutions and longer scan durations may be needed to discern differences between the signals from different regions. Physiological monitoring will be needed to determine the effect of respiratory and aliased cardiac signal on these results [51].

There are many differences between the acquisition of the 3T and 4T datasets which may account for the differences between the maps. First, the higher field strength of the 4T data may have provided the increased spatial signal to noise required to differentiate between activations in regions to allow for separation into multiple maps, while the 3T data included all of the signal changes into one map. Second, the longer scan time at 4T and more brain volumes collected per subject may have increased the temporal signal to noise which also aided in separating the clusters. Third, the music playing and the pulsed sound of the gradients at 4T, where the acquisition was only about 2/3 of the total TR, may have created pulsing activation of auditory, visual and other attention and sensory cortices across the brain as indicated in 4T map #1 of 4 (Figure 2B). However, the general similarities between the maps increase confidence in the results.

Conclusions

In this study, we identified spontaneous, coherent, transient BOLD signal changes at rest in regions of two known neural networks that have not been previously identified in the resting state using neuroimaging alone. Positive and negative BOLD signal changes were found in regions of the alpha circuit including the thalamus, precuneus and the occipital cortex. We also found positive and negative BOLD signal changes in the reticular formation. Irregular significant activation of these networks provides additional evidence supporting the hypothesis of dynamic functional networks in the resting brain [5,13,45,46]. This activity should be considered in interpreting fMRI results which use resting baselines for comparisons, especially those incorporating event-related paradigms. Further investigations are required to understand the cellular and chemical mechanisms that produce and control these signals.

Acknowledgements

Source of support: This work was supported in part by the Epilepsy Foundation (VLM), NIH EB00046 (VLM), NIH R01 1NS055822 (VLM), NIH K23 NS052468 (JPS) and the Neuroscience Institute in Cincinnati (JPS)

REFERENCES

1. Hyder F. Neuroimaging with calibrated FMRI. Stroke 2004;35(11 Suppl1):2635–41. [PubMed: 15388903]
2. Shulman RG, Rothman DL, Behar KL, Hyder F. Energetic basis of brain activity: implications for neuroimaging. Trends Neurosci 2004;27(8):489–95. [PubMed: 15271497]
3. Newman SD, Twieg DB, Carpenter PA. Baseline conditions and subtractive logic in neuroimaging. Hum Brain Mapp 2001;14(4):228–35. [PubMed: 11668654]
4. Stark CEL, Squire LR. When zero is not zero: The problem of ambiguous baseline conditions in fMRI. Proc Natl Acad Sci USA 2001;98(22):12760–65. [PubMed: 11592989]
5. Fox MD, Snyder AZ, Zacks JM, Raichle ME. Coherent spontaneous activity accounts for trial-to-trial variability in human evoked brain responses. Nature Neuroscience 2006;9(1):23–25.
6. Gonzalez-Hernandez JA, Cespedes-Garcia Y, Campbell K, et al. A pre-task resting condition neither 'baseline' nor 'zero'. Neurosci Lett 2005;391(l2):43–47. [PubMed: 16165274]
7. Mazoyer B, Zago L, Mellet E, et al. Cortical networks for working memory and executive functions sustain the conscious resting state in man. Brain Research Bulletin 2001;54(3):287–98. [PubMed: 11287133]
8. Obrig H, Neufang M, Wenzel R, et al. Spontaneous low frequency oscillations of cerebral hemodynamics and metabolism in human adults. Neuroimage 2000;12(6):623–39. [PubMed: 11112395]
9. Thompson J, Peterson M, Freeman R. Single-neuron activity and tissue oxigenation in the cerebral cortex. Science 2003;299:1070–72. [PubMed: 12586942]
10. Lowe MJ, Mock BJ, Sorenson JA. Functional connectivity in single and multislice echoplanar imaging using resting-state fluctuations. Neuroimage 1998;7(2):119–32. [PubMed: 9558644]
11. Hampson M, Olson IR, Leung HC, et al. Changes in functional connectivity of human MT/V5 with visual motion input. Neuroreport 2004;15(8):1315–19. [PubMed: 15167557]
12. Bokde AL, Tagamets MA, Friedman RB, Horwitz B. Functional interactions of the inferior frontal cortex during the processing of words and word-like stimuli. Neuron 2001;30(2):609–17. [PubMed: 11395018]
13. Fransson P. Spontaneous low-frequency BOLD signal fluctuations: An fMRI investigation of the resting-state default mode of brain function hypothesis. Hum Brain Mapp 2005;26(1):15–29. [PubMed: 15852468]
14. Fox MD, Snyder AZ, Vincent JL, et al. The human brain is intrinsically organized into dynamic, anticorrelated functional networks. Proc Natl Acad Sci USA 2005;102(27):9673–78. [PubMed: 15976020]
15. Newton AT, L. MV, Gore JC. Task demand modulation of steady-state functional connectivity to primary motor cortex. Hum Brain Mapp 2007;28:663–72. [PubMed: 17080441]
16. Lowe MJ, Phillips MD, Lurito JT, et al. Multiple sclerosis: low-frequency temporal blood oxygen level-dependent fluctuations indicate reduced functional connectivity initial results. Radiology 2002;224(1):184–92. [PubMed: 12091681]
17. Li SJ, Li Z, Wu G, et al. Alzheimer Disease: evaluation of a functional MR imaging index as a marker. Radiology 2002;225(1):253–59. [PubMed: 12355013]
18. Calhoun, VD.; Adali, T.; Hansen, LK., et al. ICA of functional MRI data: an overview; 4th International Symposium on ICA and Blind Separation; Nara, Japan. 2003.
19. De Luca M, Beckmann CF, De Stefano N, et al. fMRI resting state networks define distinct modes of long-distance interactions in the human brain. Neuroimage 2000;29(4):1359–67. [PubMed: 16260155]
20. Damoiseaux JS, Rombouts SARB, Barkhof F, et al. Consistent resting-state networks across healthy subjects. Proc Natl Acad Sci USA 2006;103(37):13848–53. [PubMed: 16945915]
21. Kiviniemi V, Kantola JH, Jauhiainen J, et al. Independent component analysis of nondeterministic fMRI signal sources. Neuroimage 2003;19(2):253–60. [PubMed: 12814576]
22. Raichle ME, MacLeod AM, Snyder AZ, et al. A default mode of brain function. Proc Natl Acad Sci USA 2001;98(2):676–82. [PubMed: 11209064]

23. Greicius MD, Krasnow B, Reiss AL, Menon V. Functional connectivity in the resting brain: a network analysis of the default mode hypothesis. Proc Natl Acad Sci USA 2003;100(1):253–58. [PubMed: 12506194]
24. Lu N, Shan BC, Li K, et al. Improved temporal clustering analysis method for detecting multiple response peaks in fMRI. J Magn Reson Imaging 2006;23(3):285–90. [PubMed: 16456825]
25. Liu Y, Gao JH, Liu HL, Fox PT. The temporal response of the brain after eating revealed by functional MRI. Nature 2000;405(6790):1058–62. [PubMed: 10890447]
26. Gao JH, Yee SH. Iterative temporal clustering analysis for the detection of multiple response peaks in fMRI. Magn Reson Imaging 2003;21(1):51–53. [PubMed: 12620546]
27. Zhao X, Glahn D, Tan LH, et al. Comparison of TCA and ICA techniques in fMRI data processing. J Magn Reson Imaging 2004;19(4):397–402. [PubMed: 15065162]
28. Morgan VL, Price RR, Arain A, et al. Resting functional MRI with temporal clustering analysis for localization of epileptic activity without EEG. Neuroimage 2004;21(1):473–81. [PubMed: 14741685]
29. Morgan VL, Gore JC, Abou-Khalil B. Cluster analysis detection of functional MRI activity in temporal lobe epilepsy. Epilepsy Res 2007;76(1):22–33. [PubMed: 17646086]
30. Morgan VL, Li Y, Abou-Khalil B, Gore JC. Development of 2dTCA for the detection of irregular, transient BOLD activity. Hum Brain Mapp 2008;29(l):57–69. [PubMed: 17290367]
31. Brett M, Johnsrude IS, Owen AM. The problem of functional localization in the human brain. Nature Reviews Neuroscience 2002;3(3):243–49.
32. Cox RW, Hyde JS. Software tools for analysis and visualization of fMRI data. NMR Biomed 1997;10 (45):171–78. [PubMed: 9430344]
33. Krasnow B, Tamm L, Greicius MD, et al. Comparison of fMRI activation at 3 and 1.5 T during perceptual, cognitive, and affective processing. Neuroimage 2003;18(4):813–26. [PubMed: 12725758]
34. Kruger G, Kastrup A, Glover GH. Neuroimaging at 1.5 T and 3.0 T: comparison of oxygenation-sensitive magnetic resonance imaging. Magn Reson Med 2001;45(4):595–604. [PubMed: 11283987]
35. Steriade M, Gloor P, Llinas RR, et al. Basic Mechanisms of Cerebral Rhythmic Activities. Electroencephalography and Clinical Neurophysiology 1990;76(6):481–508. [PubMed: 1701118]
36. Basar E, Schurmann M, BasarEroglu C, Karakas S. Alpha oscillations in brain functioning: An integrative theory. Int J Psychophysiol 1997;26(13):5–29. [PubMed: 9202992]
37. Alper KR, John ER, Brodie J, et al. Correlation of PET and qEEG in normal subjects. Psychiatry Research-Neuroimaging 2006;146(3):271–82.
38. Larson CL, Davidson RJ, Abercrombie HC, et al. Relations between PET-derived measures of thalamic glucose metabolism and EEG alpha power. Psychophysiology 1998;35(2):162–69. [PubMed: 9529942]
39. Lindgren KA, Larson CL, Schaefer SM, et al. Thalamic metabolic rate predicts EEG alpha power in healthy control subjects but not in depressed patients. Biological Psychiatry 1999;45(8):943–52. [PubMed: 10386175]
40. Sadato N, Nakamura S, Oohashi T, et al. Neural networks for generation and suppression of alpha rhythm: A PET study. Neuroreport 1998;9(5):893–97. [PubMed: 9579686]
41. Schreckenberger M, Lange-Asschenfeld C, Lochmann M, et al. Tlie thalamus as the generator and modulator of EEG alpha rhythm: a combined PET/EEG study with lorazepam challenge in humans. Neuroimage 2004;22(2):637–44. [PubMed: 15193592]
42. Moosmann M, Ritter P, Krastel I, et al. Correlates of alpha rhythm in functional magnetic resonance imaging and near infrared spectroscopy. Neuroimage 2003;20(1):145–58. [PubMed: 14527577]
43. Goldman RI, Stem JM, Engel J, Cohen MS. Simultaneous EEG and fMRI of the alpha rhythm. Neuroreport 2002;13(18):2487–92. [PubMed: 12499854]
44. Laufs H, Kleinschmidt A, Beyerle A, et al. EEG-correlated fMRI of human alpha activity. Neuroimage 2003;19(4):1463–76. [PubMed: 12948703]
45. Laufs H, Holt JL, Elfont R, et al. Where the BOLD signal goes when alpha EEG leaves. Neuroimage 2006;31(4):1408–18. [PubMed: 16537111]

46. Goncalves SI, de Munck JC, Pouwels PJW, et al. Correlating the alpha rhythm to BOLD using simultaneous EEG/fMRI: Inter-subject variabilrity. Neuroimage 2006;30(1):203–13. [PubMed: 16290018]

47. de Munck JC, Goncalves SI, Huijboom L, et al. The hemodynamic response of the alpha rhythm: An EEG/fMRI study. Neuroimage 2007;35(3):1142–51. [PubMed: 17336548]

48. Karson CN, Dykman RA, Paige SR. Blink Rates in Schizophrenia. Schizophrenia Bulletin 1990;16 (2):344–54.

49. Schurmann M, BasarEroglu C, Basar E. A possible role of evoked alpha in primary sensory processing: Common properties of cat intracranial recordings and human EEG and MEG. Int J Psychophysiol 1997;26(13):149–70. [PubMed: 9203001]

50. Feige B, Scheffler K, Esposito F, et al. Cortical and subcortical coirelates of electroencephalographic alpha rhythm modulation. J Neurophysiol 2005;93(5):2864–72. [PubMed: 15601739]

51. Birn RM, Diamond JB, Smith MA, Bandettini PA. Separating respiratory-variation-related fluctuations from neuronal-activity-related fluctuations in fMRI. Neuroimage 2006;31(4):1536–48. [PubMed: 16632379]

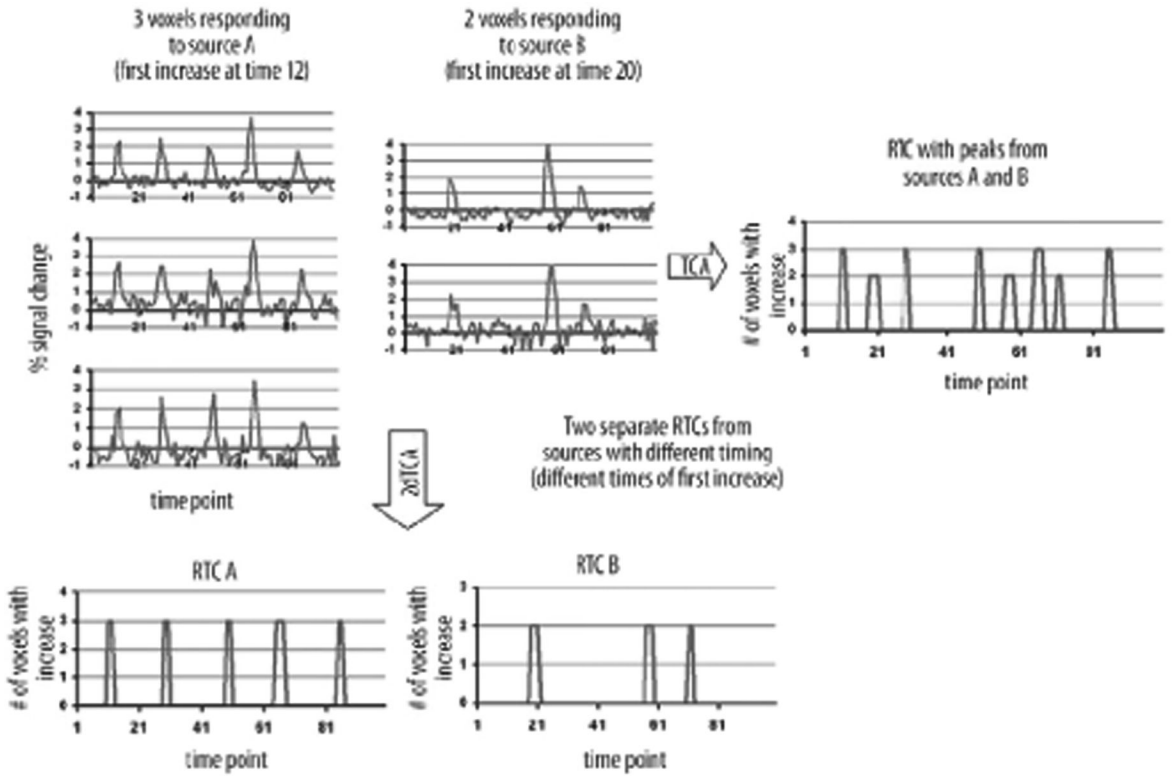

Figure 1.

Graphical depiction of the TCA and 2dTCA algorithms showing how multiple reference time courses (RTCs) are created by the 2dTCA algorithm when signalsfrom multiple sources are included in the data. Three example voxels with a similar response are shown from Source A. Two example voxels with a similar BOLD response that is different than that of Source A are shown from Source B. The RTC resulting from the TCA algorithm incorporates peaks from all five voxels, while the RTCs resulting from the 2dTCA algorithm separate the two different BOLD responses into two RTCs.

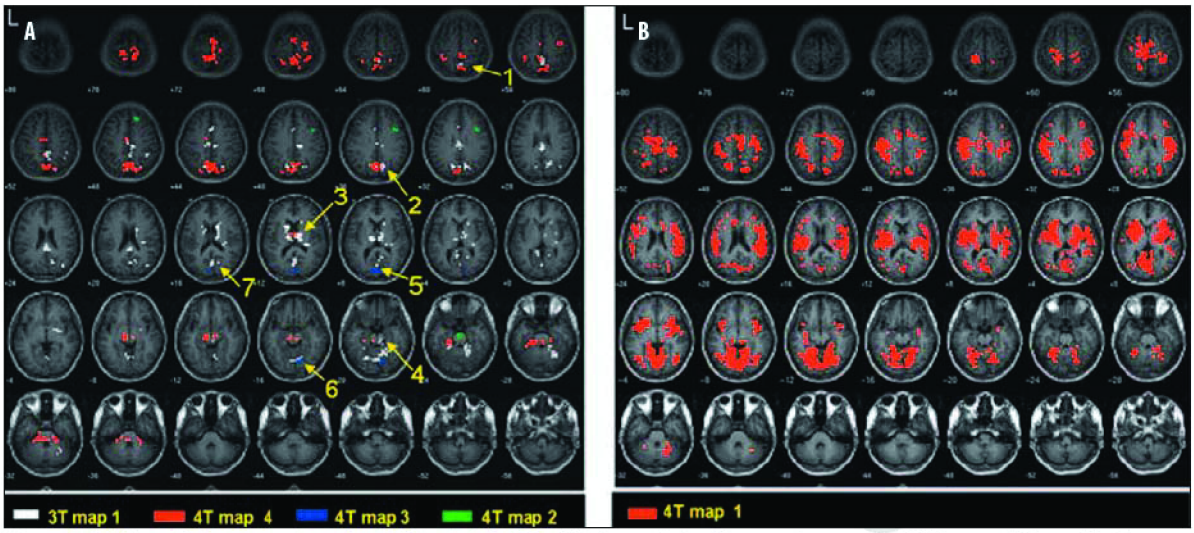

Figure 2.
Positive activation maps of transient BOLD activity in 3T and 4T datasets in healthy controls at rest ($p<0.05$, *corrected*) determined by 2dTCA. Regions of similarity between 3T and 4T results are numbered according to descriptions in Table 2. Images are in MNI coordinate space, a) 3T map #1 of 1,4T maps #2,3 and 4 of 4. b) 4T map #1 of 4.

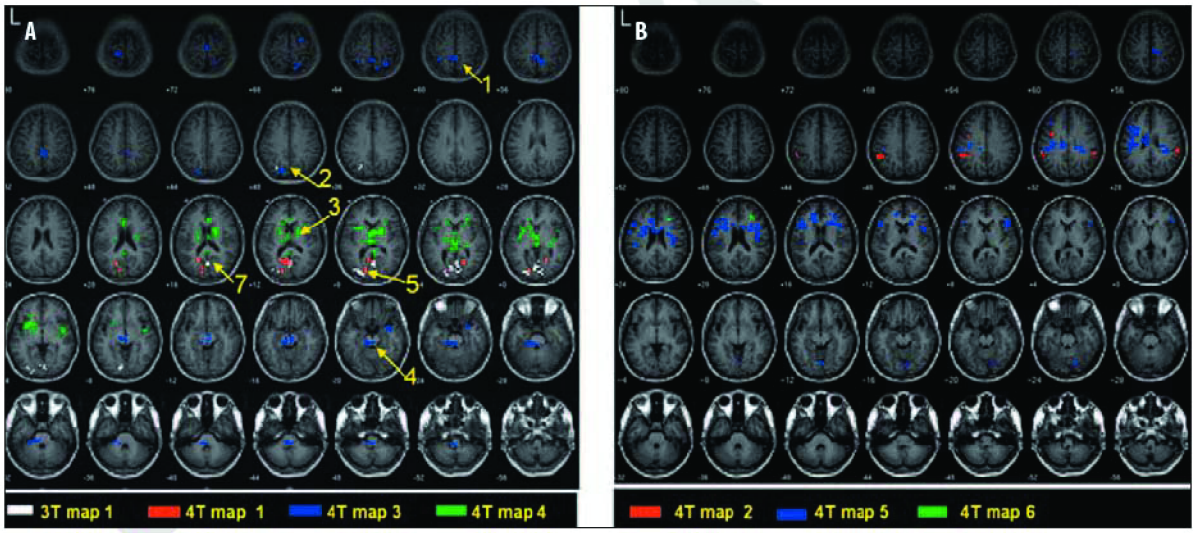

Figure 3.
Negative activation maps of transient BOLD activity in 3T and 4T datasets in healthy controls at rest ($p<0.05$, *corrected*) determined by 2dTCA. Regions of similarity between 3T and 4T results are numbered according to descriptions in Table 2. Images are in MNI coordinate space, a) 3T map #1 of 1,4T maps #1,3 and 4 of 6. b) 4T maps #2,5, and 6 of 6.

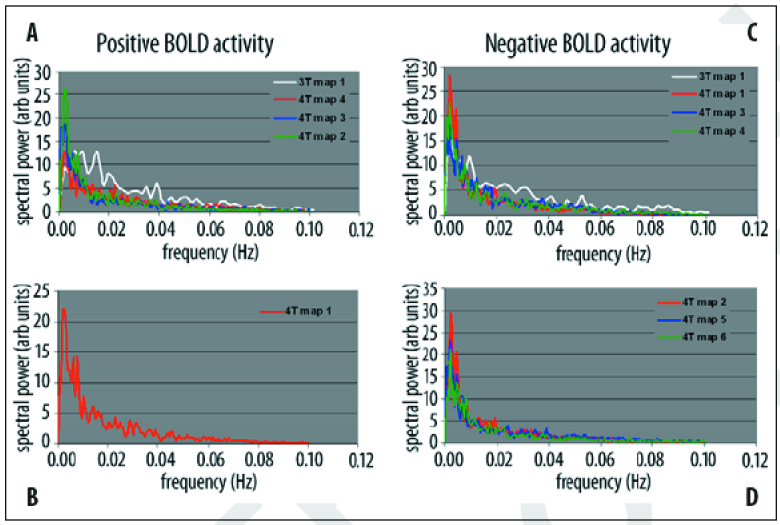

Figure 4.

Average spectral power of transient BOLD activity in healthy controls at rest ($p<0.05$, *corrected*). a and b) Positive BOLD activity. Line colors correspond to map colors in Figures 2A and 2B, Cand D. Negative BOLD activity. Line colors correspond to map colors in Figures 3A and 3B. Only frequencies up to 0.10 Hz are shown to highlight region of most power.

Table 1

FMRI image acquisition parameters for 3T and 4T datasets

	3T	4T
Echotime-TE(msec)	25	30
Repetition time - TR (msec)	2000	3000
Image acquisition time - TA (msec)	1988	1800
In-plane resolution (mm)	3.75×3.75	4×4
Number of slices	30	30
Slice thickness/gap (mm)	4.5/0.5	4.0/0.0
#Volumes	200	396
Scan time (min)	6.7	19.8
EEG acquired?	No	Yes
Eyes closed?	Yes	Yes
Music played?	No	Yes
Other fMRI data collected?	Yes	No

Table 2

Similar regions of coherent positive and negative BOLD signal changes in BT and 4T datasets determined by 2dTCA

Region#	Positive activation		Negative activation		Region description	MNI coordinates
	3Tmap#	4Tmap#	3Tmap#	4Tmap#		
1	1	4		3	Inferior parietal lobe, BA 40	-364-460
2	1	1,4	1	3	Parietal lobe, precuneus	127-636
3	1	4		4	Thalamus	12881-2
4	1	2,4		3	Brainstemandpons	82-42-0
5	1	1,3	1	1	Occipital lobe	89-28
6	1	1,3			Cerebellum	126-86-
7	1	1	1	1	Posterior cingulate	-405-616

Region number corresponds to numbers indicated in Figures 2A and 3A. MNI coordinates indicate center of one comparable activated duster in this region.